

# We are IntechOpen, the world's leading publisher of Open Access books Built by scientists, for scientists

6,900

Open access books available

186,000

International authors and editors

200M

Downloads

Our authors are among the

154

Countries delivered to

TOP 1%

most cited scientists

12.2%

Contributors from top 500 universities



WEB OF SCIENCE™

Selection of our books indexed in the Book Citation Index  
in Web of Science™ Core Collection (BKCI)

Interested in publishing with us?  
Contact [book.department@intechopen.com](mailto:book.department@intechopen.com)

Numbers displayed above are based on latest data collected.  
For more information visit [www.intechopen.com](http://www.intechopen.com)



---

# Wall Conduction Effects in Laminar Counterflow Parallel-Plate Heat Exchangers with Small-Scale Wall Corrugations

---

Marcos Vera and Alberto E. Quintero

Additional information is available at the end of the chapter

<http://dx.doi.org/10.5772/60550>

---

## 1. Introduction

Parallel-plate heat exchangers are widely used in chemical, pharmaceutical, food processing, and many other industrial applications. More recently, they have also found application in a variety of emerging branches of thermal engineering. They are currently used in miniaturized reaction systems involving heterogeneously catalyzed gas-phase reactions [1], in thermoelectric generators that convert low-grade thermal energy into electrical power [2, 3], and in thermoacoustic engines [4]. In addition, they are a key component of many cryogenic systems [5,6,7].

Progress in the analysis of parallel-plate heat exchangers has been significant in the last decades due to their simple geometry and well established flow conditions [8]. In particular, the analysis of the steady-state laminar heat transfer between different streams coupled through compatibility conditions at the boundaries constitutes the so-called conjugated Graetz problem. Under certain simplifying assumptions, i.e., constant property fluids and fully developed laminar flow, the problem becomes linear and is amenable to an elegant solution based on eigenfunction expansions, which in counterflow systems involves sets of positive and negative eigenfunctions associated with sets of positive and negative eigenvalues [9,10,11,12].

It is well known that the use of corrugated plates is a suitable method for increasing the thermal performance of heat exchangers and provide higher compactness [13]. In many practical applications the flow is turbulent, and the corrugated surface has a significant effect on the enhancement of heat transfer rates. Because of the presence of highly unsteady recirculation zones, the heat transfer coefficients obtained with corrugated walls are higher than those with flat plates. However, the pressure drop is also significantly higher.

In some other cases the Reynolds number remains small due to the small dimensions of the system, hence laminar flow conditions prevail. In this case the corrugation troughs exhibit low-velocity swirling cells [14] that are both weak and steady. As a result, the convective heat enhancement process is poor and the effect on heat exchanger performance is much smaller. For certain corrugation shapes and/or flow conditions no enhancement of the heat transfer rate may even occur [15]. Thus, even if the heat transfer surface between the wall and the fluid is increased, the global heat transfer effectiveness may not overcome that of a flat wall channel of comparable size [16]. This difficulty has motivated a considerable amount of work on methods to increase the rates of heat and mass transfer in compact heat exchangers operated in the laminar flow regime.

Durmuş et al. [17] demonstrated that under laminar flow conditions the heat exchanged by a plate heat exchanger with a corrugated sinusoidal surface is higher than for other geometries (flat plate and asterisk plate), although corrugated plate heat exchangers exhibit also higher pressure drops. Specifically, the pressure drop in corrugated channels is higher than in flat channels of the same external size. Therefore, a trade-off exists between the heat gained and the pressure drop, because increasing the heat exchanger efficiency leads to smaller system dimensions, which reduces production costs, whereas larger pressure drops result in increased operating costs.

The aim of this work is to extend recent analyses of laminar counterflow parallel-plate heat exchangers [12,18,19] to quantify the effect of small scale wall corrugations. In particular, the amplitude and wavelength of the corrugations will be assumed to be comparable to each other, but small compared to the channel half-widths. Although such separation of scales hardly occurs in practical devices, it enables the problem to be solved by a multi-scale asymptotic approach similar to that proposed by Woollard et al. [20] for mass transfer in channels with small-scale wall corrugations. In this case the problem exhibits two main asymptotic regions: a bulk flow region where the walls appear flat at leading order, and a wall region where there is a full interaction between convection and conduction in the fluids, coupled by transverse and longitudinal conduction in the (thin) corrugated wall.

The multi-scale asymptotic analysis proceeds in two steps:

- On the large (i.e., bulk flow) scale, a theoretical study of laminar counterflow parallel-plate heat exchangers [19] provides the temperature field as an infinite series of eigenfunctions associated with sets of positive and negative eigenvalues. The analysis, which ignores the effects of axial conduction both in the fluids and in the plates, is used to construct an approximate two-term solution that incorporates the effect of higher order eigenfunctions through apparent temperature offsets introduced at the inlet/outlet sections [12]. The approximate solution yields an accurate description of the temperature field away from the thermal entrance regions, thereby enabling simplified expressions for the wall and fluid temperatures, local Nusselt numbers, and overall heat-transfer coefficient in terms of the wall thermal resistance.
- On the small (i.e., wall corrugation) scale, the shear-induced flow of two Newtonian fluids that exchange heat through a thin corrugated wall is studied numerically, retaining both transverse and longitudinal conduction effects in the heat conducting wall. The analysis shows that far from the wall the effect of the corrugations is equivalent to that of a thickened

virtual plane surface with partial slip along the corrugations [21,22]. This virtual plane wall exhibits an apparent thermal resistance that incorporates i) the intrinsic thermal resistance of the corrugated wall, ii) an additional resistance due to the apparent wall thickening, and iii) a negative contribution associated with the heat-transfer enhancement induced by the corrugations (due to the enlarged heat exchange surface area and, when the wall conductivity is larger than those of the fluids, also to the longitudinal heat conduction along the wall). Apparent wall thicknesses and thermal resistances will be presented here for the reference case of sinusoidal corrugations.

Evaluating the approximate solution of the bulk flow model presented in Section 2 with the apparent thermal resistance derived from the wall corrugation model of Section 3, a physically sound multi-scale description of laminar counterflow parallel-plate heat exchangers with small-scale wall corrugations is proposed in Section 4. Illustrative results are presented in Section 5, and some conclusions are drawn in Section 6.

## 2. Bulk flow model

In this section we analyze the heat exchange process between two constant-property fluids flowing through a multilayered counterflow parallel-plate heat exchanger composed by a relatively large number of channels. A detailed account of this problem can be found elsewhere [19], but we shall summarize here its main aspects for completeness of the presentation. The flow channels are separated by flat plates of finite thickness,  $\delta_w$ , and thermal conductivity,  $k_w$ . The heat conducting plates allow the exchange of heat through a section of length  $L$ . Figure 1 shows a sketch of the theoretical configuration under study, showing the coordinate system, the velocity profiles, the boundary conditions, and the physical properties of fluids  $i = 1, 2$  (namely, fluid density,  $\rho_i$ , heat capacity,  $c_i$  and thermal conductivity,  $k_i$ ).

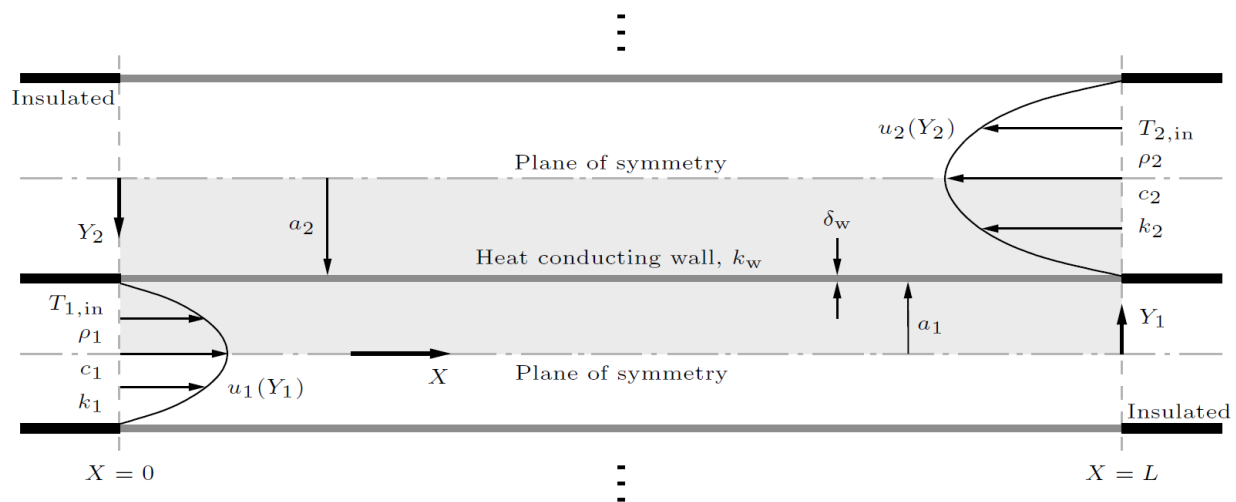


**Figure 1.** Unitary cell of the idealized counterflow parallel-plate heat exchanger considered in the bulk flow model, showing the coordinate system, the velocity profiles, the inlet conditions, and the physical properties of fluids 1 and 2. A heat conducting wall, of finite thickness,  $\delta_w$  and thermal conductivity,  $k_w$ , separates both fluids. The domain under study is shaded gray.

The Reynolds numbers,  $Re_i = 2a_i V_i / \nu_i$ , based on the channel half-width,  $a_i$ , average flow velocity,  $V_i$ , and kinematic viscosity,  $\nu_i$ , of fluid  $i$ , are assumed to be sufficiently small for the flows to remain laminar and steady [23]. The Prandtl numbers,  $Pr_i = \nu_i / \alpha_i$ , based on the thermal diffusivity,  $\alpha_i = k_i / (\rho_i c_i)$ , of fluid  $i$ , are also assumed to be moderately large compared to unity, a good approximation for most non-metallic liquids in applications. In this case, the thermal entry length is large compared to the hydrodynamic entry length, and the flow can be assumed to be a fully developed Poiseuille flow independent of the temperature field,  $u_i(Y_i) = \pm(3/2)V_i[1 - (Y_i/a_i)^2]$ , where the + (–) sign holds for fluid 1 (2). As a result, we shall assume that the Peclet numbers of the flow in the channels,  $Pe_i = Re_i Pr_i = 2a_i V_i / \alpha_i$ , are both large compared to unity. Then, axial heat conduction can be neglected in both fluids in first approximation, and we can assume that the inlet temperature of fluid  $i$  is uniform and equal to  $T_{i,in}$ .

To write the problem in non-dimensional form, we introduce the dimensionless axial and transverse coordinates  $\xi = X/(Pe_1 a_1)$  and  $y_i = Y_i/a_i$ , and the normalized temperature  $\theta_i = (T_i - T_{1,in}) / (T_{2,in} - T_{1,in})$ . Then, under the assumptions stated above, the energy equation reduces, in first approximation, to a balance between axial convection and transverse conduction

$$\begin{aligned} \frac{3}{4}(1-y_1^2) \frac{\partial \theta_1}{\partial \xi} &= \frac{\partial^2 \theta_1}{\partial y_1^2} \\ -m \frac{3}{4}(1-y_2^2) \frac{\partial \theta_2}{\partial \xi} &= \frac{\partial^2 \theta_2}{\partial y_2^2} \end{aligned} \quad \text{in } 0 < \xi < \xi_L, \quad 0 < y_i < 1. \quad (1)$$

These equations are to be integrated with adiabatic boundary conditions at the channel symmetry planes

$$\frac{\partial \theta_1}{\partial y_1} = \frac{\partial \theta_2}{\partial y_2} = 0 \quad \text{at } 0 < \xi < \xi_L, \quad y_i = 0, \quad (2)$$

the condition of continuity of wall-normal heat fluxes at the heat conducting wall

$$\begin{aligned} \theta_2 - \theta_1 &= \frac{1}{\kappa_w} \frac{\partial \theta_1}{\partial y_1} = \frac{\nu(\xi)}{\kappa_w} \\ \frac{\partial \theta_1}{\partial y_1} &= -k \frac{\partial \theta_2}{\partial y_2} \equiv \nu(\xi) \end{aligned} \quad \text{at } 0 < \xi < \xi_L, \quad y_i = 1, \quad (3)$$

and the inlet conditions

$$\begin{aligned} \theta_1 &= \theta_{1,in} = 0 \quad \text{at } \xi = 0, \quad 0 \leq y_1 < 1, \\ \theta_2 &= \theta_{2,in} = 1 \quad \text{at } \xi = \xi_L, \quad 0 \leq y_2 < 1. \end{aligned} \quad (4)$$

It should be noted that in writing the compatibility condition at the heat conducting wall (3) we have ignored the effect of axial conduction in the wall, which constitutes a good approximation provided the dimensionless wall thickness  $\delta_w/a_1$  remains sufficiently small [19].

The solution to the problem stated above provides the temperature field,  $\theta_i(\xi, y_i)$ , for given values of the parameters

$$m = \frac{a_2 \text{Pe}_2}{a_1 \text{Pe}_1}, \quad k = \frac{a_1 k_2}{a_2 k_1}, \quad \kappa_w = \frac{a_1 k_w}{\delta_w k_1}, \quad \text{and} \quad \xi_L = \frac{L}{a_1 \text{Pe}_1}. \quad (5)$$

It also provides the local heat-transfer rate from fluid 2 to fluid 1,  $v(\xi)$ , the interfacial wall-fluid temperature distributions,  $\theta_{wi}(\xi) \equiv \theta_i(\xi, 1)$ , the local wall temperature jump,  $\theta_{w2}(\xi) - \theta_{w1}(\xi) = v(\xi)/\kappa_w$ , and the outlet temperature profiles,  $\theta_{1,\text{out}}(y_1) = \theta_1(\xi_L, y_1)$  and  $\theta_{2,\text{out}}(y_2) = \theta_2(0, y_2)$ . Another interesting result is the spatial distribution of the bulk (or mixing-cup) temperatures

$$\theta_{mi}(\xi) = \int_0^1 \frac{3}{2} (1 - y_i^2) \theta_i(\xi, y_i) dy_i \quad (6)$$

which represent the uniform temperature that would eventually be attained by fluid  $i$  if it was allowed to evolve adiabatically downstream of a certain section  $\xi$ . This includes, in particular, the values of the outlet bulk temperatures of both streams,  $\theta_{m1}(\xi_L) \equiv \theta_{m1,\text{out}}$  and  $\theta_{m2}(0) \equiv \theta_{m2,\text{out}} = 1 - \theta_{m1,\text{out}}/(mk)$ , which are closely related to the heat exchanger effectiveness [12].

It is interesting to note that the inverse of  $\kappa_w$ , which appears explicitly in Eq. (3) represents the dimensionless wall thermal resistance,  $1/\kappa_w = (\delta_w/a_1)/(k_w/k_1)$ , defined as the ratio of the dimensionless wall thickness,  $\delta_w/a_1$ , to the dimensionless heat conductivity,  $k_w/k_1$ ; the dimensionless wall temperature jump being proportional to  $1/\kappa_w$ . Note also that the product of  $m$  and  $k$  represents the ratio of heat capacity flow rates,  $mk = (2a_2 V_2 \rho_2 c_2)/(2a_1 V_1 \rho_1 c_1)$ , which will hereafter be assumed, without loss of generality, to be greater than one, so that fluid 1 has the lowest heat capacity flow rate [12].

Following standard practice, the solution of the problem can be expanded as an infinite series of eigenfunctions of the form [19]

$$\theta_i(\xi, y_i) = A + \sum_{n=-\infty}^{+\infty} C_n e^{-\lambda_n \xi} g_{n,i}(y_i) \quad (7)$$

where the eigenfunctions are given by

$$g_{n,i}(y_i) = \left( 1 \mp \frac{g'_{n,1}(1)}{2\kappa_w} \right) f_{n,i}(y_i), \quad g'_{n,1}(1) = \frac{f'_{n,1}(1)}{1 + \frac{1}{2\kappa_w} f'_{n,1}(1)} \quad (8)$$

with the  $- (+)$  sign corresponding to fluid 1 (2), and the eigenvalues are determined by the eigencondition

$$f'_{n,1}(1; \lambda_n) + k f'_{n,2}(1; m, \lambda_n) \left[ 1 + \frac{f'_{n,1}(1; \lambda_n)}{\kappa_w} \right] = 0. \quad (9)$$

In the above expressions,  $f_{n,i}(y_i)$  represent the eigenfunctions of the thermally thin wall limit  $\kappa_w \rightarrow \infty$  (or  $1/\kappa_w \rightarrow 0$ ) which can be expressed in terms of Whittaker functions as shown by Vera & Liñán [12]. These written can be derived analytically and evaluated at  $y_i = 1$  to give the derivative of the eigenfunctions at the heat conducting wall

$$f'_{n,i}(1) = -\frac{1}{2} + 2 \left[ \kappa_{n,i} + \frac{2\sqrt{\pi} \left( \frac{3}{4} + \kappa_{n,i} \right) M_{\kappa_{n,i}+1, \frac{1}{4}}(4\kappa_{n,i}) - \Gamma \left( \frac{1}{4} - \kappa_{n,i} \right) W_{\kappa_{n,i}+1, \frac{1}{4}}(4\kappa_{n,i})}{2\sqrt{\pi} M_{\kappa_{n,i}, \frac{1}{4}}(4\kappa_{n,i}) + \Gamma \left( \frac{1}{4} - \kappa_{n,i} \right) W_{\kappa_{n,i}, \frac{1}{4}}(4\kappa_{n,i})} \right], \quad (10)$$

where  $\kappa_{n,1} = \sqrt{3\lambda_n}/8$ ,  $\kappa_{n,2} = i\sqrt{3m\lambda_n}/8$ ,  $\Gamma(z)$  is the complex Gamma function and  $i$  is the imaginary unit. Using this expression in Eq. (9) it is possible to compute the eigenvalues  $\lambda_n$  for given values of  $m$ ,  $k$ , and  $\kappa_w$ .

As pointed out by Nunge and Gill [9], the exact solution to the problem stated in Eqs. (1) – (4) involves an infinite set of linear equations for the coefficients  $A$  and  $C_n$  involved in the series expansion (7), which must be truncated to a finite number of terms in order to get an approximate numerical solution. An alternative approach, initially proposed by Vera and Liñán [12] in the thermally thin wall limit and recently extended by Quintero et al. [19] to the case of non-zero wall thermal resistance, proceeds by constructing an approximate two-term solution that retains only the first two eigenvalues (0 and  $\lambda_0$ ) but still incorporates the effect of higher order terms through apparent temperature offsets  $\Delta_i$  at the inlet section of fluid  $i$ . This leads to analytic expressions for the outlet bulk temperatures of the form

$$\begin{aligned} \theta_{m1,\text{out}} &\cong \Delta_1 + (1 - \Delta_1 - \Delta_2) \left[ \frac{1 - e^{-\lambda_0 \xi_L}}{1 - (mk)^{-1} e^{-\lambda_0 \xi_L}} \right] + mk \Delta_2 \\ \theta_{m2,\text{out}} &\cong \Delta_1 + (1 - \Delta_1 - \Delta_2) \left[ \frac{1 - (mk)^{-1}}{1 - (mk)^{-1} e^{-\lambda_0 \xi_L}} \right] + (mk)^{-1} \Delta_1 \end{aligned} \quad (11)$$

where  $\Delta_i$  represents the inlet bulk temperature offset of fluid  $i$  associated with the neglected higher-order eigenfunctions at both ends of the heat exchanger, given by

$$\Delta_1 = \left[ \frac{1 - (mk)^{-1}}{1 - (mk)^{-1} e^{-\lambda_0 \xi_L}} \right] \frac{\Delta_1^{[0]}}{2}, \quad \Delta_2 = (mk)^{-1} \left[ 1 - \frac{1 - e^{-\lambda_0 \xi_L}}{1 - (mk)^{-1} e^{-\lambda_0 \xi_L}} \right] \frac{\Delta_1^{[0]}}{2} \quad (12)$$

with

$$\Delta_1^{[0]} = \frac{2(1 + mk)g'_{0,1}{}^2(1) + mk \left[ \Omega_0^- - \frac{g'_{0,1}(1)\Omega_0^+}{2\kappa_w} \right] \lambda_0^2}{8g'_{0,1}{}^2(1) + (1 + mk) \left[ \Omega_0^- - \frac{g'_{0,1}(1)\Omega_0^+}{2\kappa_w} \right] \lambda_0^2}. \quad (13)$$

For given values of  $m$ ,  $k$ ,  $\kappa_w$ , and  $\xi_L$ , the above expressions provide closed-form approximate expressions for the outlet bulk temperatures of both streams in terms of the computed values of  $\lambda_0$ ,  $g'_{0,1}(1)$ , and

$$\Omega_0^\pm = \frac{\partial}{\partial \lambda_0} \left[ g'_{0,1}(1; \lambda_0) \pm kg'_{0,2}(1; m, \lambda_0) \right], \quad (14)$$

which are to be obtained numerically from Eqs. (8) – (10). As shown by Quintero et al. [19], the approximate two-term solution provides accurate representations for the temperature field away from the thermal entrance regions, thereby enabling simplified expressions for the wall and bulk temperature distributions, local Nusselt numbers, and overall heat-transfer coefficient.

Figure 2 shows the variation of the outlet bulk temperature of fluid 1,  $\theta_{m1,out}$  with the dimensionless wall thermal resistance,  $1/\kappa_w$  for increasing values of the heat exchanger length,  $\xi_L = [0.125, 0.25, 0.5, 1, 2]$ . As previously discussed, although  $m$  and  $k$  take different values in the left and right plots, in both cases  $mk = (\dot{m}_2 c_2) / (\dot{m}_1 c_1) > 1$ , so that  $\theta_{m1,out}$  coincides by definition with the heat exchanger effectiveness.

The model results indicate that the heat exchanger effectiveness increases monotonously with the dimensionless heat exchanger length,  $\xi_L$ , and decreases with the wall thermal resistance,  $1/\kappa_w$ . The results presented in Figure 2 were obtained from the numerical integration of Eqs. (1) – (4) (solid lines) and from the approximate two-term solution presented above (symbols). As can be seen, the agreement is excellent even for the shortest heat exchangers under study, with errors below 1% for  $\xi_L \geq 0.25$  [19]. This demonstrates that the approximate two-term solution constitutes a fast evaluation tool that could be readily used for the optimization of heat exchanger performance.

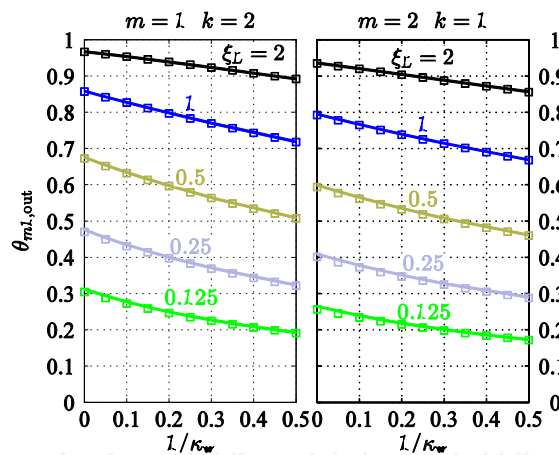


**Figure 2.** Variation of the outlet bulk temperature of fluid 1 with the wall thermal resistance  $1/\kappa_w$  for several heat exchanger lengths  $\xi_L$  corresponding to  $m = 1, k = 2$  (left) and  $m = 2, k = 1$  (right), as obtained from the numerical integration of Eqs. (1) – (4) (solid lines) and from the approximate two-term solution (symbols).

The aim of the following sections is to extend the present analysis to the study of laminar counterflow heat exchangers with small-scale wall corrugations. It will be shown that when the corrugation wavelength and amplitude are small compared to the channel half-widths, the effect of the corrugated wall on the bulk flow is similar to that of a thickened virtual plane surface with an apparent thermal resistance that has to be obtained numerically. We shall begin in Section 3 investigating the local conjugate heat-transfer problem that provides this apparent thermal resistance for a fixed wall design, characterized by its shape, thickness, and thermal conductivity, and specified values of the Reynolds and Prandtl numbers of both streams. The

analysis will provide the apparent values of the dimensionless parameters  $m^*$ ,  $k^*$ ,  $\kappa_w^*$ , and  $\xi_L^*$  that should be used in the bulk flow model to incorporate the effect of small-scale wall corrugations and evaluate the corresponding changes in heat exchanger performance.

### 3. Wall corrugation model

In this section, we analyze the incompressible two-dimensional shear-induced flow of two constant property fluids  $i = 1, 2$ , that exchange heat through a thin corrugated wall. The wall thickness,  $\delta_w$ , is assumed to be small compared to the corrugation wavelength,  $\lambda$ , so that the dimensionless wall thickness,  $\Delta_w = \delta_w / \lambda \ll 1$ , emerges naturally as a small parameter. In addition, the Reynolds numbers of the shear flows at both sides of the wall,  $Re_{\tau_i} = \rho_i \lambda^2 \tau_i / \mu_i^2$ , based on the shear stress far from the wall,  $\tau_i$ , the corrugation wavelength,  $\lambda$ , and the fluid density,  $\rho_i$  and viscosity,  $\mu_i$ , of fluid  $i$ , are also assumed to be sufficiently small for the flows to remain laminar and steady.

The mathematical formulation of the problem can be written in non-dimensional form using the corrugation wavelength  $\lambda$  as appropriate length scale. The resulting Cartesian dimensionless coordinates  $(x, y, z)$  are shown in Figure 3. The wall geometry is assumed to be a periodic function of the  $x$ -coordinate, while the  $y$ -coordinate is defined normal to the mean plane of the corrugated wall pointing from fluid 1 to fluid 2. The  $z$ -coordinate is perpendicular to the  $x$ - $y$  plane shown in the figure.

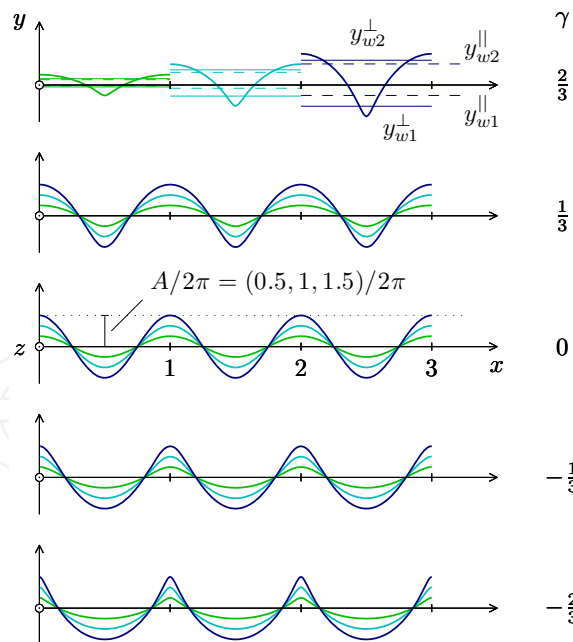


**Figure 3.** Schematic representation of the wall geometry defined by the functions  $x_w(\alpha)$  and  $y_w(\alpha)$  given by Eq. (15). The upper plot illustrates the apparent wall position for Stokes flow (i.e.,  $Re_i=0$ ) parallel ( $y_{wi}^{\parallel}$ , dashed lines) and transverse ( $y_{wi}^{\perp}$ , solid lines) to the corrugations for the three corrugation amplitudes  $A/2\pi = [0.5, 1, 1.5]/2\pi$  considered in the figure.

For illustrative purposes, we define the corrugation shape using the parametric representation

$$x = x_w(\alpha) = \frac{\alpha + \gamma \sin(\alpha)}{2\pi}, \quad y = y_w(\alpha) = \frac{A}{2\pi} \cos(\alpha), \quad \alpha \in \mathbb{R}, \quad (15)$$

adopted from [24]. Here,  $A \geq 0$  measures the amplitude of the corrugations,  $A/2\pi$  being an effective amplitude-to-wavelength ratio, and  $-1 \leq \gamma \leq 1$  represents a suitable scallop parameter. As previously discussed, we further assume that the dimensionless wall thickness is small,  $\Delta_w \ll 1$ , as often occurs in the applications. The surface thus defined is periodic and symmetric with respect to  $x$ , with the  $x$ -axis located midway between the highest and lowest points of the corrugations, and with values of  $y_w(\alpha)$  ranging between  $\pm A/2\pi$ . The parameter  $\gamma$  has a strong influence on the corrugation shape. Thus, for  $\gamma = 0$  the surface adopts a wavy (i.e., sinusoidal) shape devoid of any irregularities, whereas for  $0 < |\gamma| < 1$  it develops a scalloped geometry that becomes more and more pronounced for increasing values of  $|\gamma|$ , with downward (upward) cusps appearing in the surface as  $\gamma \rightarrow 1$  ( $-1$ ). Note that the amplitude parameter  $A$  also represents the maximum slope of the sinusoidal surface  $y_w = (A/2\pi)\cos(2\pi x)$  obtained for  $\gamma = 0$ .

The velocity of fluid  $i$  is measured with the characteristic shear velocity  $\lambda\tau_i/\mu_i$  to give the dimensionless velocity field  $\mathbf{u} = (u, v, w)$ . The variations in pressure with respect to its unperturbed value far from the wall are scaled in fluid  $i$  with the corresponding shear stress,  $\tau_i$  to give the dimensionless pressure,  $p$ . Finally, the characteristic temperature  $q\lambda/k_1$ , based on the corrugation wavelength,  $\lambda$ , the heat conductivity of fluid 1,  $k_1$ , and the overall heat flux,  $q$ , transferred from fluid 2 to fluid 1, is used to define the dimensionless temperature  $T$ . Note that the thermal coupling through the heat conducting wall enforces the use of a common temperature scale for both fluids.

Assuming that the pressure, velocity, and temperature fields are translation invariant along the  $z$ -axis, the continuity, momentum, and energy conservation equations take the form

$$\begin{aligned} \frac{\partial u}{\partial x} + \frac{\partial v}{\partial y} &= 0 \\ \text{Re}_{ti} \left( u \frac{\partial u}{\partial x} + v \frac{\partial u}{\partial y} \right) &= -\frac{\partial p}{\partial x} + \frac{\partial^2 u}{\partial x^2} + \frac{\partial^2 u}{\partial y^2} \\ \text{Re}_{ti} \left( u \frac{\partial v}{\partial x} + v \frac{\partial v}{\partial y} \right) &= -\frac{\partial p}{\partial y} + \frac{\partial^2 v}{\partial x^2} + \frac{\partial^2 v}{\partial y^2} \\ \text{Re}_{ti} \left( u \frac{\partial w}{\partial x} + v \frac{\partial w}{\partial y} \right) &= \frac{\partial^2 w}{\partial x^2} + \frac{\partial^2 w}{\partial y^2} \\ \text{Re}_{ti} \text{Pr}_i \left( u \frac{\partial T}{\partial x} + v \frac{\partial T}{\partial y} \right) &= \frac{\partial^2 T}{\partial x^2} + \frac{\partial^2 T}{\partial y^2} \end{aligned} \quad (16)$$

where viscous dissipation has been neglected in the energy balance and  $\text{Pr}_i = \nu_i/\alpha_i = \mu_i/(k_i/c_i)$  denotes again the Prandtl number of fluid  $i$ . The above equations must be integrated in the periodic domain  $0 < x < 1$  for fluids 1 and 2, located, respectively, below ( $-\infty < y < y_w^-$ ) and above

( $y_w^+ < y < \infty$ ) the wall. Hereafter we shall use  $y_w$  to denote the wall position,  $y_w^\pm$  representing the lower (-) and upper (+) wall surfaces.

As boundary conditions we impose periodicity at  $x=0$  and 1, the no-slip boundary condition at the wall

$$y = y_w : \quad u = v = w = 0, \quad (17)$$

and a uniform shear flow far from the wall

$$y \gg 1: \quad \frac{\partial u}{\partial y} = \sin \theta_2, \quad v = 0, \quad \frac{\partial w}{\partial y} = \cos \theta_2, \quad p = 0, \quad (18)$$

$$-y \gg 1: \quad \frac{\partial u}{\partial y} = -\sin \theta_1, \quad v = 0, \quad \frac{\partial w}{\partial y} = -\cos \theta_1, \quad p = 0. \quad (19)$$

In the far field boundary conditions  $\theta_i$  denotes the angle of misalignment between the wall corrugations and the uniform shear imposed on fluid  $i$  far from the wall. So that  $\theta_i=0, \pi$ , and  $\theta_i = \pm\pi/2$  correspond, respectively, to flows parallel ( $u = v = p = 0$ ) and transverse ( $w = 0$ ) to the corrugations, with  $\theta_2 = \theta_1$  and  $\theta_2 = \theta_1 + \pi$  corresponding, respectively, to co-current and counter-current flow arrangements.

We also impose the overall heat flux transferred by conduction from fluid 2 to fluid 1 by specifying a uniform temperature gradient in fluid 2 far from the wall

$$y \gg 1: \quad \frac{\partial T}{\partial y} = K^{-1}, \quad (20)$$

where  $K = k_2/k_1$  denotes the fluid-to-fluid heat conductivity ratio, whereas in fluid 1 we impose a linear temperature profile of the form

$$-y \gg 1: \quad T = y. \quad (21)$$

Note that, due to the invariance of the problem under arbitrary shifts in temperature, we can always add a constant to the temperature distribution of fluid 1 so as to set its apparent value at the mean plane ( $y = 0$ ) of the corrugated wall equal to zero.

In the thin wall limit considered here,  $\Delta_w \ll 1$ , the jump conditions for the temperature and the wall-normal heat fluxes at the heat conducting wall can be written as

$$y = y_w : \quad \begin{cases} T_w^+ - T_w^- = \frac{\Delta_w}{K_w} \left[ \frac{v_w^+ + v_w^-}{2} + \mathcal{O}(\Delta_w^2) \right] \\ v_w^+ - v_w^- = -\Delta_w K_w \left[ \frac{1}{2} \left( \frac{d^2 T_w^+}{ds^2} + \frac{d^2 T_w^-}{ds^2} \right) + \mathcal{O}(\Delta_w^2) \right] \end{cases} \quad (22)$$

where  $T_w^\pm = T(x_w(\alpha), y_w^\pm(\alpha))$  denotes the temperature at the upper (+) and lower (-) wall surfaces, and

$$v_w^+ = K \frac{\partial T(x_w(\alpha), y_w^+(\alpha))}{\partial n}, \quad v_w^- = \frac{\partial T(x_w(\alpha), y_w^-(\alpha))}{\partial n} \quad (23)$$

are the local wall-normal heat fluxes transferred by conduction from fluid 2 to the wall, and from the wall to fluid 1, respectively. In the above expressions,  $n$  represents the local wall-normal coordinate pointing from fluid 1 to fluid 2, and  $s$  is the arc-length coordinate measured along the wall, defined by

$$ds = \sqrt{x_w'^2(\alpha) + y_w'^2(\alpha)} d\alpha. \quad (24)$$

In addition to the dimensionless wall thickness,  $\Delta_w$ , the jump conditions (22) involve the wall-to-fluid heat conductivity ratio,  $K_w = k_w/k_l$ , as an additional dimensionless parameter; the wall temperature difference being proportional to  $\Delta_w/K_w$ , whereas the jump in wall-normal heat fluxes is proportional to  $\Delta_w K_w$ . As a result, in the formal limit  $\Delta_w \rightarrow 0$  both  $\Delta_w$  and  $K_w$  disappear from the formulation and the jump conditions (22) reduce to the continuity of temperatures,  $T_w^+ = T_w^-$ , and wall-normal heat fluxes,  $v_w^+ = v_w^-$ .

Inspection of the mathematical problem stated above shows that the steady conjugate heat transfer between two shear-induced flows separated by a corrugated wall can be characterized by the Reynolds and Prandtl numbers of the two fluid streams,  $Re_{\tau_i}$  and  $Pr_i$ , the fluid-to-fluid and wall-to-fluid heat conductivity ratios,  $K = k_2/k_1$  and  $K_w = k_w/k_l$ , the dimensionless wall thickness,  $\Delta_w = \delta_w/\lambda \ll 1$ , the angles of misalignment between the imposed shear and the direction of the corrugations,  $\theta_i$ , and the dimensionless wall geometry, determined here by the parameters  $A$  and  $\gamma$ . Thus, for a fixed wall geometry the solution of the problem depends on the nine dimensionless parameters:  $Re_{\tau_1}$ ,  $Re_{\tau_2}$ ,  $Pr_1$ ,  $Pr_2$ ,  $K$ ,  $K_w$ ,  $\Delta_w$ ,  $\theta_1$ , and  $\theta_2$ .

In addition to the velocity, pressure, and temperature fields, the solution of the problem determines the virtual no-slip plane wall location for the flows parallel ( $y_{wi}^{\parallel}$ ) and transverse ( $y_{wi}^{\perp}$ ) to the corrugations

$$\begin{aligned} y_{w2}^{\parallel} &= \lim_{y \rightarrow \infty} \left( y - \frac{w}{\cos \theta_2} \right), & y_{w2}^{\perp} &= \lim_{y \rightarrow \infty} \left( y - \frac{u}{\sin \theta_2} \right), \\ y_{w1}^{\parallel} &= \lim_{y \rightarrow -\infty} \left( y + \frac{w}{\cos \theta_1} \right), & y_{w1}^{\perp} &= \lim_{y \rightarrow -\infty} \left( y + \frac{u}{\sin \theta_1} \right), \end{aligned} \quad (25)$$

as well as the apparent temperature jump at  $y = 0$

$$\Delta T = \lim_{y \rightarrow \infty} (T - K^{-1}y). \quad (26)$$

The conjugate heat transfer problem stated in Eqs. (16) – (22) can be solved numerically using standard finite-difference or finite-volume methods. A closer inspection reveals that the transverse flow problem ( $u, v, p$ ) is uncoupled from the longitudinal flow ( $w$ ) and thermal ( $T$ ) problems, so that it can be integrated first; the resulting velocity field being required to evaluate the convective terms in the equations for  $w$  and  $T$ . Since the transverse flow field is two-

dimensional, a vorticity-streamfunction formulation was adopted for the numerical integration, thereby avoiding the determination of the pressure field, which is not required here. Fourth-order finite differences were used for the spatial discretization, resulting in a five-point explicit scheme. An algebraic non-orthogonal coordinate transformation was previously employed to map the complex fluid domain onto a square computational domain with uniform grid spacing, thereby enabling a simple treatment of the wall curvilinear boundaries. The far field boundary conditions (18) – (21) were imposed sufficiently far from the wall to ensure the independence of the solution on the size of the numerical domain. The solution was then marched in pseudo-time until a converged (i.e., steady) solution was obtained. A grid independence study was carried out to ensure at least 4 significant digits in the reported values of  $y_{wi}^{\parallel}$ ,  $y_{wi}^{\perp}$  and  $\Delta T$ .

Although the formulation presented above is of great generality, the large number of parameters involved makes unfeasible a thorough parametric study. As a result, the analysis will be restricted here to the case of two-dimensional counter-current flows,  $\theta_2 = -\theta_1 = \pi/2$ , transverse to sinusoidal corrugations,  $\gamma = 0$ . Figure 4 presents illustrative results for  $Pr_i = 5$ ,  $K = 2$ ,  $K_w = 0.1$ ,  $\Delta_w = 0.1$ ,  $A = 1$ , and different values of  $Re_{ti} = [32, 128, 512]$ . As can be seen, the flow exhibits the typical low-velocity recirculation regions within the corrugation troughs, which grow spatially with the Reynolds number. The presence of this quasi-stagnant fluid in the vicinity of the wall modifies the overall wall thermal resistance, thereby changing the effectiveness of the heat exchange process in a way that is to be determined below.

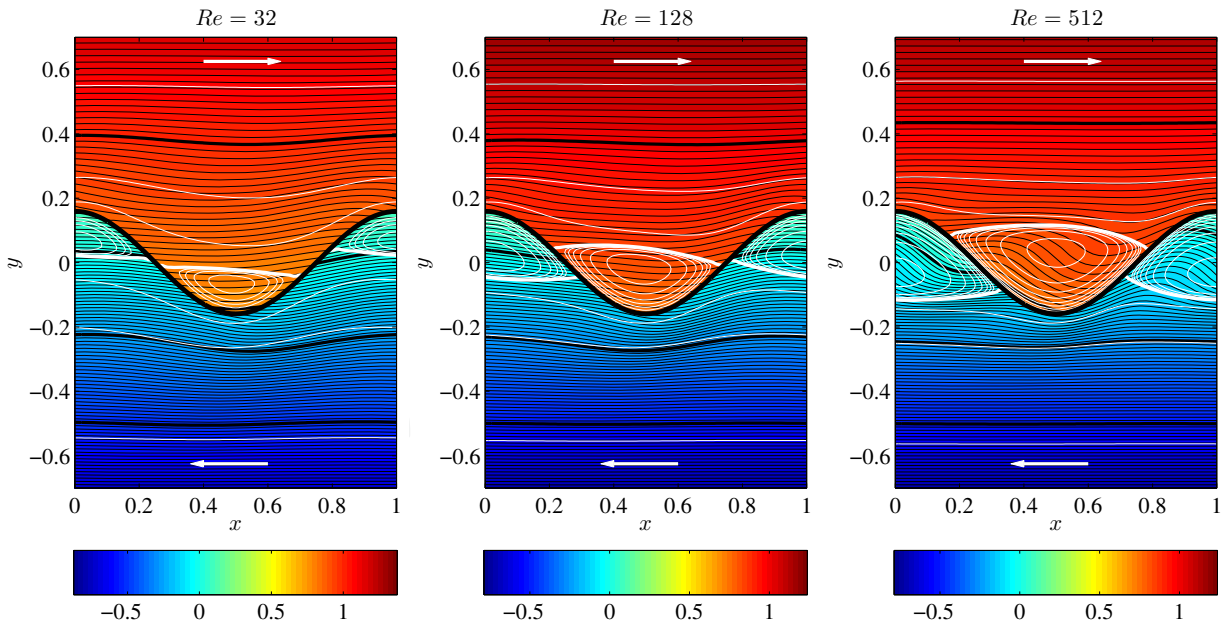


**Figure 4.** Streamlines (white contours) obtained for  $A = 1$ ,  $\gamma = 0$ ,  $\theta_2 = -\theta_1 = \pi/2$ , and  $Re_{ti} = [32, 128, 512]$ , and temperature field (black contours and colored background; see colorbars for the color scale) corresponding to  $Pr_i = 5$ ,  $K = 2$ ,  $K_w = 0.1$ , and  $\Delta_w = 0.1$ . The parameters defining the thickened virtual plane surface, obtained from the three simulations shown in the figure, are  $y_{w2}^{\perp} = -y_{w1}^{\perp} = [0.1032, 0.1084, 0.1167]$  and  $\Delta T = [0.8092, 0.8081, 0.7688]$ .

Figure 5 top shows the effect of the Reynolds number on the virtual no-slip plane wall location for flow transverse to the corrugations,  $y_{wi}^{\perp}$ , given by Eq. (25). As can be seen, the growth of

the recirculation regions observed in Figure 4 results in an apparent thickening of the virtual plane wall for increasing values of  $Re_{\tau_i}$ . On the other hand, for decreasing  $Re_{\tau_i}$  the value of  $y_{wi}^\perp$  approaches the asymptotic (i.e., Stokes-flow) limit provided by the semi-analytical solution of Luchini et al. [25], recalculated here as an additional check of the accuracy of the numerical method. Figure 5 (bottom) shows the influence of the Reynolds number  $Re_{\tau_i}$  on the apparent temperature jump  $\Delta T$  at  $y = 0$ , defined by Eq. (26). As can be seen, for low wall conductivities  $\Delta T$  takes positive values due to the correspondingly large wall thermal resistance. However, for high wall conductivities  $\Delta T$  becomes negative due to the effect of longitudinal heat conduction along the wall, which provides an efficient way of transferring heat from the corrugation crests to the troughs, making the wall to behave as an effective thermal shortcut. This mechanism, which is absent for  $K_w \ll 1$ , becomes dominant for  $K_w \gg 1$ , leading to the negative values of  $\Delta T$  reported in the last plot of Figure 5. It is also interesting to note that although  $\Delta T$  tends to decrease for increasing values of  $Re_{\tau_i}$  due to the enhancement of heat transfer by convection, in poorly conductive walls this trend is partially reversed for  $Re_{\tau_i}$  in the range 100 – 200, when the downstream stagnation points of the swirling cells that develop at each side of the wall come closer to each other; see, e.g, Figure 4.

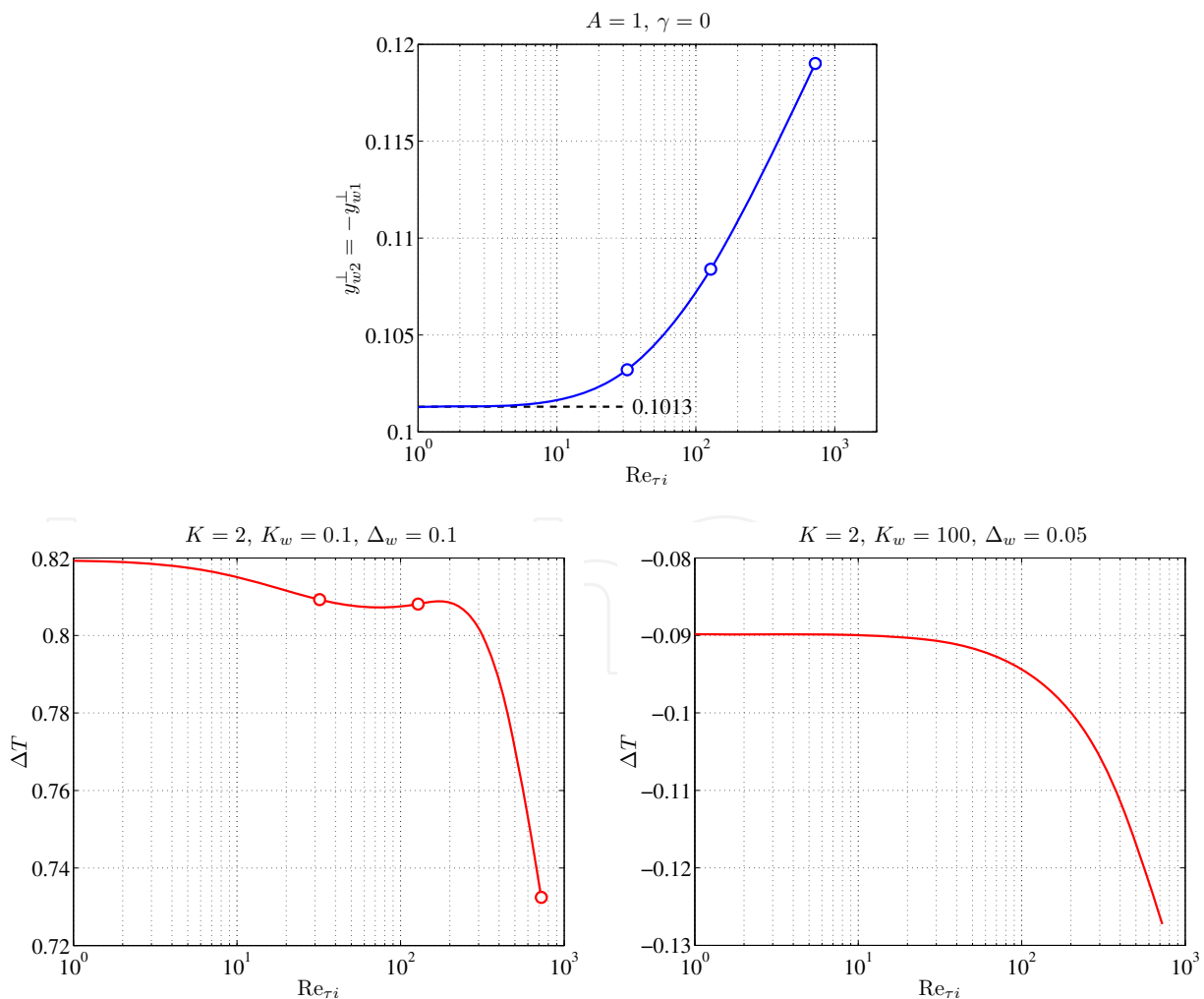


**Figure 5.** Top: Variation with the Reynolds number of the apparent plane wall location for flow transverse to the corrugations obtained numerically for  $A = 1, \gamma = 0$ . Bottom: Variation with the Reynolds number of the normalized apparent

wall temperature jump  $\Delta T$  for values of  $Pr_i = 5$ ,  $K$ ,  $K_w$  and  $\Delta_w$  representative of low (left) and high (right) conductive walls. The open symbols indicate values obtained from the simulations of Figure 4.

#### 4. Combined multi-scale model

The virtual plane wall concept introduced in Section 3 can be used in numerical simulations of corrugated-plate, or –tube, heat exchangers to account for the effect of small-scale wall corrugations in a computationally effective way. According to the results presented above, the corrugated wall behaves as a virtual plane wall of apparent thickness

$$\Delta_w^* = y_{w2}^\perp + \Delta_w - y_{w1}^\perp > \Delta_w, \quad (27)$$

with an apparent wall temperature jump

$$\Delta T^* = K^{-1}y_{w2}^\perp + \Delta T - y_{w1}^\perp > \Delta T. \quad (28)$$

This virtual wall separates two fluid channels of apparent half-widths

$$a_i^* = a_i - \lambda |y_{w,i}^\perp| = a_i \left( 1 - \frac{\lambda}{a_i} |y_{w,i}^\perp| \right) < a_i, \quad (29)$$

smaller than the average channel half-widths,  $a_i$ , as a result of the apparent wall displacement introduced by the corrugations, which effectively reduces the hydraulic diameter of the channels. From here on, all apparent quantities obtained from the application of the virtual plane wall concept will be denoted by a superscript asterisk (\*).

Note that the dimensionless corrugation wavelength,  $\Lambda_i = \lambda/a_i$ , appearing explicitly in Eq. (29) must be small compared to unity for the present multi-scale asymptotic analysis to hold. Otherwise the flow perturbations induced by the corrugations would significantly alter the flow in the channels, which will no longer resemble a planar Poiseuille flow, as assumed in Section 2.

Using Eq. (29) to evaluate the apparent channel half-widths, we obtain the apparent value of parameter

$$k^* = \frac{k_2 a_1^*}{k_1 a_2^*} = \frac{k_2 a_1}{k_1 a_2} \left( \frac{a_1^* / a_1}{a_2^* / a_2} \right) = k \frac{\left( 1 - \frac{\lambda}{a_1} |y_{w,1}^\perp| \right)}{\left( 1 - \frac{\lambda}{a_2} |y_{w,2}^\perp| \right)}. \quad (30)$$

The apparent value of  $\kappa_w^* = (k_w / \delta_w)^* (a_1^* / k_1)$  can be determined from the dimensional apparent wall temperature jump  $(q\lambda / k_1)\Delta T^*$ , where  $\Delta T^*$  is given by Eq. (28) in terms of the computed

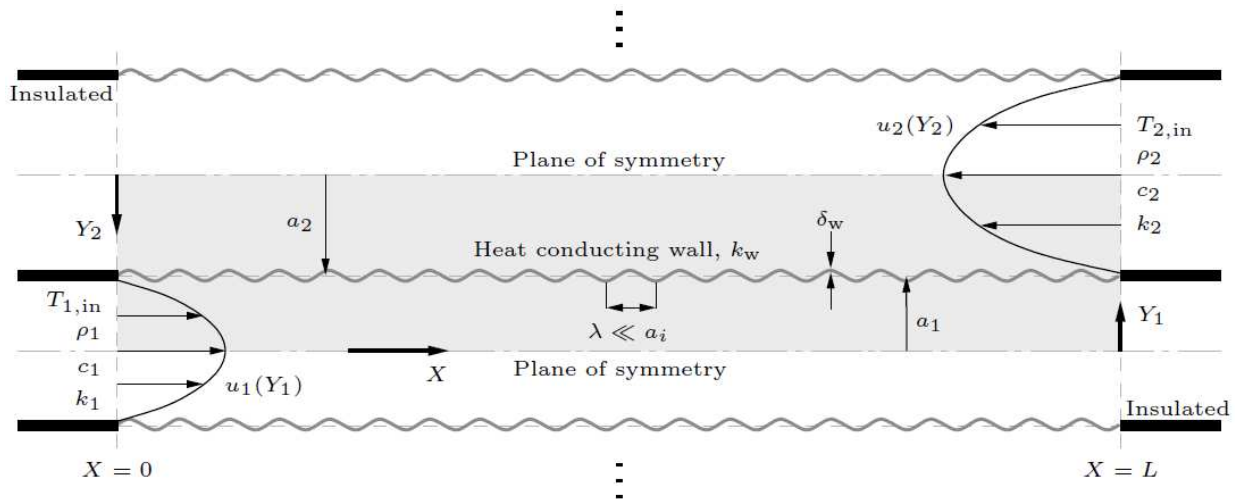


**Figure 6.** A corrugated heat conducting wall of finite thickness,  $\delta_w$  and thermal conductivity,  $k_w$  separates the channels of fluids 1 and 2 with average half-widths  $a_1$  and  $a_2$ , respectively. The wall corrugation amplitude and wavelength are both assumed to be small compared to  $a_i$ .

values of  $y_{wi}^\perp$  and  $\Delta T$ . Multiplying the apparent wall temperature jump by  $(k_w/\delta_w)^* = \kappa_w^*(k_1/a_1^*)$  we should recover the overall heat flux transferred by conduction from fluid 2 to fluid 1, i.e.,  $q = (q\lambda/k_1)\Delta T^* \kappa_w^*(k_1/a_1^*)$ , whence solving for  $\kappa_w^*$  we get

$$\kappa_w^* = \frac{a_1^*}{\lambda \Delta T^*} = \frac{a_1}{\lambda \Delta T^*} \left( 1 - \frac{\lambda}{a_1} |y_{w,1}^\perp| \right) = \underbrace{\left( \frac{a_1}{\delta_w} \frac{k_w}{k_1} \right)}_{\kappa_w} \underbrace{\left( \frac{\delta_w}{\lambda} \frac{k_1}{k_w} \right)}_{\Delta_w/K_w} \frac{1}{\Delta T^*} \left( 1 - \frac{\lambda}{a_1} |y_{w,1}^\perp| \right) = \frac{\kappa_w}{\Delta T^*} \left( 1 - \frac{\lambda}{a_1} |y_{w,1}^\perp| \right). \quad (31)$$

In the above expression we have expressed  $\kappa_w^*$  in terms of the normalized apparent wall temperature jump

$$\overline{\Delta T} = \frac{\Delta T^*}{\Delta_w / K_w} \quad (32)$$

a quantity defined so that it tends to unity as the amplitude of the corrugations tends to zero ( $A \rightarrow 0$ ). In this limiting case, when  $y_{w,1}^\perp$  also tends to zero, Eq. (31) reduces to  $\kappa_w^* = \kappa_w \equiv (k_w/\delta_w)(a_1/k_1)$ , and the original expression for  $\kappa_w$  given in Eq. (5) for a flat wall of finite thickness,  $\delta_w$ , and thermal conductivity,  $k_w$ , is recovered. Note also that, by definition, the values of  $\kappa_w$ ,  $K_w$ ,  $\Delta_w \ll 1$ , and  $\Lambda \ll 1$  verify the following relation

$$\kappa_w = \frac{a_1}{\delta_w} \frac{k_w}{k_1} = \frac{a_1}{\lambda} \frac{\lambda}{\delta_w} \frac{k_w}{k_1} = \frac{K_w}{\Lambda \Delta_w} \quad (33)$$

which provides  $\kappa_w$  explicitly in terms of  $K_w$ ,  $\Delta_w$  and  $\Lambda$ .

Figure 7 shows the influence of the Reynolds number,  $Re_{\tau_i}$  on the normalized apparent wall temperature jump,  $\overline{\Delta T}$ , for the same values of  $K$ ,  $K_w$  and  $\Delta_w$  considered in Figure 5. As can be seen, for low-conductive walls  $\overline{\Delta T}$  remains slightly below unity regardless of the Reynolds number. In this case, the relatively high conductivity of the recirculating fluids combined with the higher surface area of the corrugated wall results in a smaller apparent wall temperature jump as compared to the originally flat wall. On the other hand, for high-conductive walls  $\overline{\Delta T}$  takes values well above unity, indicating that in this case the presence of low-conductive recirculating fluids within the corrugation troughs significantly increases the apparent wall temperature jump. In both cases,  $\overline{\Delta T}$  exhibits a non-monotonous behavior with  $Re_{\tau_i}$  that ends in an abrupt reduction for Reynolds numbers  $Re_{\tau_i}$  above 300 or so.

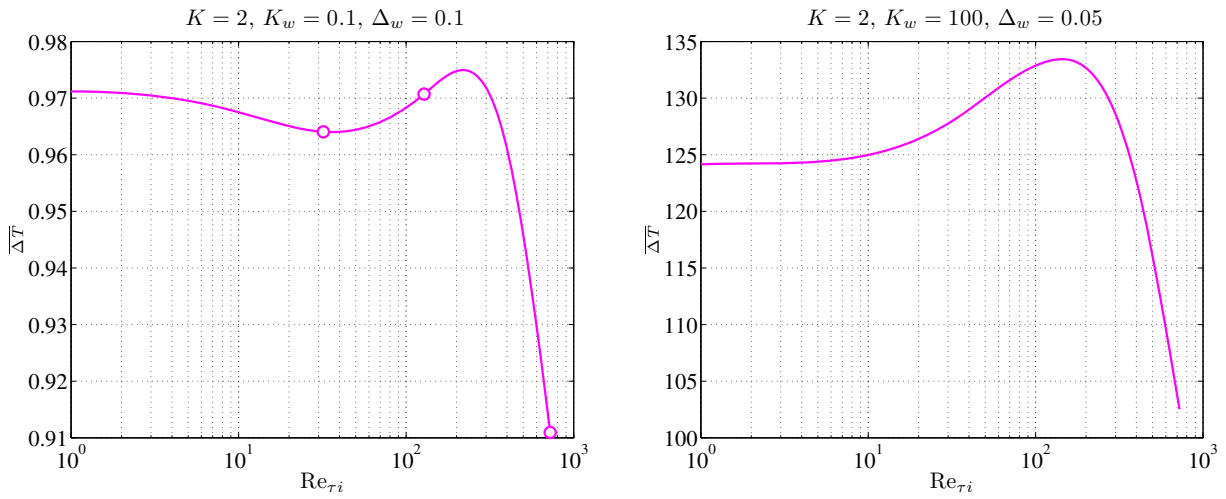


**Figure 7.** Variation with the Reynolds number of the normalized apparent wall temperature jump  $\overline{\Delta T}$  for values of  $Pr_i = 5$ ,  $K$ ,  $K_w$  and  $\Delta_w$  representative of low (left) and high (right) conductive walls. The open symbols correspond to results obtained from the simulations of Figure 4.

For the plane Poiseuille flow considered in this work, the wall shear stress is given by  $\tau_i = 3\mu_i V_i / a_i$ , which upon substitution in the expression for  $Re_{\tau_i}$  yields the relation

$$Re_{\tau_i} = \frac{\rho_i \lambda^2 \tau_i}{\mu_i} = \frac{3}{2} \left( \frac{\lambda}{a_i} \right)^2 \frac{2\rho_i V_i a_i}{\mu_i} = \frac{3}{2} \Lambda_i^2 Re_i, \quad (34)$$

stating that the ratio between the Reynolds numbers  $Re_{\tau_i}$  and  $Re_i$  equals 3/2 times the square of the dimensionless wall corrugation wavelength,  $\Lambda_i = \lambda/a_i \ll 1$ . Since in plane Poiseuille flow finite-amplitude disturbances are known to drive transition to turbulence at Reynolds numbers as low as  $Re_{i,crit} \cong 1330$  [23], the above expression severely limits the maximum value of  $Re_{\tau_i}$  compatible with steady laminar flow in the channels. Thus, for the moderately large value of  $\Lambda_i$  considered below ( $\Lambda_i = 0.25 \ll 1$ ) the maximum allowable value of  $Re_{\tau_i}$  turns out to

be 125. From the results shown in Figure 7, it is clear that below this critical Reynolds number the normalized wall temperature jump  $\overline{\Delta T}$  remains almost constant, with convective effects accounting only for small variations of  $\overline{\Delta T}$  of order 1% for  $K_w = 0.1$  and 7% for  $K_w = 100$ . Thus, to get a first idea of the effect of the corrugations on the performance of the heat exchanger we may simply evaluate  $\kappa_w^*$  using Eq. (31) with the value of  $\overline{\Delta T}$  corresponding to  $Re_{\tau_i} = 0$ .

To quantify this effect, let us consider the ratio between the overall heat transfer rate,  $\dot{m}c_1(T_{m1,out} - T_{1,in})$ , and the mechanical power required to drive the flow, characterized here by the pumping power,  $\Delta P_1 Q_1$ , delivered to fluid 1. Normalizing this ratio with that of a flat-wall heat exchanger, we introduce the overall augmentation heat-transfer number

$$R_a = \frac{\left[ \frac{\dot{m}_1 c_1 (T_{m1,out} - T_{1,in})}{\Delta P_1 Q_1} \right]_{\text{corr}}}{\left[ \frac{\dot{m}_1 c_1 (T_{m1,out} - T_{1,in})}{\Delta P_1 Q_1} \right]_{\text{flat}}}, \quad (35)$$

where  $T_{m1,out}$  denotes the outlet bulk temperature of fluid 1. As previously discussed, this temperature is closely related to the heat exchanger effectiveness,  $\varepsilon = (T_{m1,out} - T_{1,in}) / (T_{2,in} - T_{1,in})$ , when fluid 1 has the smallest heat capacity flow rate. For the plane Poiseuille flow considered in this work the pressure drop,  $\Delta P_i$ , the volume flow rate,  $Q_i$ , and the mass flow rate,  $\dot{m}$ , are given respectively by

$$\Delta P_i = \frac{3\mu_i V_i}{a_i^2} L, \quad Q_i = 2a_i V_i, \quad \dot{m}_i = \rho_i Q_i. \quad (36)$$

Using these expressions in Eq. (35), the overall augmentation heat-transfer number can be expressed as

$$R_a = \left( \frac{a_1^*}{a_1} \right)^2 \frac{V_1 \varepsilon^*}{V_1^* \varepsilon}. \quad (37)$$

A thorough optimization of the heat exchange process requires also comparison of the entropy generation rates achieved with corrugated and flat walls. As a first attempt to use the entropy minimization method [26,27,28] for the thermodynamic optimization of corrugated-wall heat exchangers, we introduce the augmentation entropy generation number

$$N_a = \frac{\dot{S}_{\text{corr}}}{\dot{S}_{\text{flat}}} = \frac{(\dot{S}/\dot{m}_1 c_1)_{\text{corr}} (\dot{m}_1 c_1)_{\text{corr}}}{(\dot{S}/\dot{m}_1 c_1)_{\text{flat}} (\dot{m}_1 c_1)_{\text{flat}}} = \frac{(\dot{S}/\dot{m}_1 c_1)_{\text{corr}} \left( \frac{Q_1^*}{Q_1} \right)}{(\dot{S}/\dot{m}_1 c_1)_{\text{flat}}} = \frac{(\dot{S}/\dot{m}_1 c_1)_{\text{corr}} \left( \frac{a_1^* V_1^*}{a_1 V_1} \right)}{(\dot{S}/\dot{m}_1 c_1)_{\text{flat}}} \quad (38)$$

defined as the ratio of the entropy generation rates with corrugated and flat plates. In the above expression  $\dot{S}/\dot{m}_1 c_1$  denotes the dimensionless entropy generation rate, which is approximated by

$$\begin{aligned} \frac{\dot{S}}{\dot{m}_1 c_1} &\cong \frac{\dot{S}_1 + \dot{S}_2}{\dot{m}_1 c_1} \cong \ln \frac{T_{m1,out}}{T_{1,in}} + \frac{\overbrace{\dot{m}_2 c_2}^{mk}}{\dot{m}_1 c_1} \ln \frac{T_{m2,out}}{T_{2,in}} = \ln \left[ \frac{T_{m1,out}}{T_{1,in}} \left( \frac{T_{m2,out}}{T_{2,in}} \right)^{mk} \right] \\ &= \ln \left[ \left( 1 + \varepsilon \frac{\Delta T}{T_{1,in}} \right) \left( \frac{1}{1 + \Delta T/T_{1,in}} \right)^{mk} \left( 1 + \left( 1 - \frac{\varepsilon}{mk} \right) \frac{\Delta T}{T_{1,in}} \right)^{mk} \right], \end{aligned} \quad (39)$$

where entropy changes associated with viscous dissipation (i.e., pressure drop irreversibility) and heat conduction in the wall have both been neglected. These changes should be retained in a detailed second-law analysis of heat exchanger performance, which is not to be pursued in this work, as they may be critical for the thermodynamic optimization of the heat transfer equipment [29]. It should be noted that the evaluation of the dimensionless entropy generation rate requires the introduction of the dimensionless temperature difference  $\Delta T/T_{1,in} = (T_{2,in} - T_{1,in})/T_{1,in}$  or, alternatively, the temperature ratio  $T_{2,in}/T_{1,in} = \Delta T/T_{1,in} + 1$ , as an additional parameter of the problem.

Combining Eqs. (38) and (39), we obtain the final expression for the augmentation entropy generation number

$$N_a = \frac{\ln \left[ \left( 1 + \varepsilon^* \frac{\Delta T}{T_{1,in}} \right) \left( \frac{1}{1 + \Delta T/T_{1,in}} \right)^{m^* k^*} \left( 1 + \left( 1 - \frac{\varepsilon^*}{m^* k^*} \right) \frac{\Delta T}{T_{1,in}} \right)^{m^* k^*} \right]}{\ln \left[ \left( 1 + \varepsilon \frac{\Delta T}{T_{1,in}} \right) \left( \frac{1}{1 + \Delta T/T_{1,in}} \right)^{mk} \left( 1 + \left( 1 - \frac{\varepsilon}{mk} \right) \frac{\Delta T}{T_{1,in}} \right)^{mk} \right]} \left( \frac{a_1^* V_1^*}{a_1 V_1} \right). \quad (40)$$

The remaining two apparent parameters of the bulk flow model, i.e.,  $m^*$  and  $\xi_L^*$ , involve by definition the Peclet numbers of the fluid streams. To evaluate their apparent values we must therefore specify the apparent Peclet numbers,  $Pe_i^*$ , in the heat exchanger with corrugated walls. To this end, we shall consider three different flow constraints, namely: i) constant flow rate, ii) constant pumping power, and iii) constant pressure drop.

### i. Constant flow rate

To ensure that the volume flow rate  $Q_i = 2a_i V_i$  of fluid  $i$  is the same with flat and corrugated walls, the average flow velocity  $V_i^*$  must grow to compensate for the reduction of the channel half-width

$$V_i^* a_i^* = V_i a_i \Rightarrow V_i^* = V_i \frac{a_i}{a_i^*} = V_i \left( 1 - \frac{\lambda}{a_i} |y_{w,i}^\perp| \right)^{-1}. \quad (41)$$

In this case, the apparent value of  $Pe_i$ , defined with the apparent velocities and channel half-widths, remains unchanged

$$Pe_i^* = \frac{2a_i^* V_i^*}{\alpha_i} = \frac{2a_i V_i}{\alpha_i} = Pe_i, \quad (42)$$

while the apparent values of  $m$  and  $\xi_L$  are given by

$$m^* = \frac{Pe_2^* a_2^*}{Pe_1^* a_1^*} = \frac{Pe_2 a_2}{Pe_1 a_1} \left( \frac{a_2^* / a_2}{a_1^* / a_1} \right) = m \frac{\left( 1 - \frac{\lambda}{a_2} |y_{w,2}^\perp| \right)}{\left( 1 - \frac{\lambda}{a_1} |y_{w,1}^\perp| \right)} \Rightarrow m^* k^* = mk, \quad (43)$$

$$\xi_L^* = \frac{L}{a_1^* Pe_1^*} = \frac{L}{a_1 Pe_1} \left( \frac{a_1}{a_1^*} \right) = \xi_L \left( 1 - \frac{\lambda}{a_1} |y_{w,1}^\perp| \right)^{-1}. \quad (44)$$

Using (29) and (41) in (37), the overall augmentation heat-transfer parameter takes the form

$$R_a = \left( 1 - \frac{\lambda}{a_1} |y_{w,1}^\perp| \right)^3 \frac{\varepsilon^*}{\varepsilon}. \quad (45)$$

## ii. Constant pumping power

The pumping power is equal to the product of the volume flow rate,  $2a_i V_i$ , by the pressure drop,  $3\mu_i L V_i / a_i^2$ . To ensure that the pumping power remains the same with flat and corrugated walls, the average flow velocity  $V_i^*$  of fluid  $i$  must satisfy the condition

$$\frac{V_i^{*2}}{a_i^*} = \frac{V_i^2}{a_i} \Rightarrow V_i^* = V_i \left( \frac{a_i^*}{a_i} \right)^{\frac{1}{2}} = V_i \left( 1 - \frac{\lambda}{a_i} |y_{w,i}^\perp| \right)^{\frac{1}{2}}. \quad (46)$$

In this case, the apparent values of  $Pe_i$ ,  $m$ , and  $\xi_L$  are given by

$$Pe_i^* = \frac{2a_i^* V_i^*}{\alpha_i} = \frac{2a_i V_i}{\alpha_i} \left( \frac{a_i^* V_i^*}{a_i V_i} \right) = Pe_i \left( 1 - \frac{\lambda}{a_i} |y_{w,i}^\perp| \right)^{\frac{3}{2}}, \quad (47)$$

$$m^* = m \left[ \frac{1 - \frac{\lambda}{a_2} |y_{w,2}^\perp|}{1 - \frac{\lambda}{a_1} |y_{w,1}^\perp|} \right]^{\frac{5}{2}} \Rightarrow m^* k^* = mk \left[ \frac{1 - \frac{\lambda}{a_2} |y_{w,2}^\perp|}{1 - \frac{\lambda}{a_1} |y_{w,1}^\perp|} \right]^{\frac{3}{2}}, \quad (48)$$

$$\xi_L^* = \xi_L \left( 1 - \frac{\lambda}{a_1} |y_{w,1}^\perp| \right)^{-\frac{5}{2}}, \quad (49)$$

and, using (29) and (46) in (37), the overall augmentation heat-transfer number takes the form

$$R_a = \left( 1 - \frac{\lambda}{a_1} |y_{w,1}^\perp| \right)^{\frac{3}{2}} \frac{\varepsilon^*}{\varepsilon}. \quad (50)$$

### iii. Constant pressure drop

To ensure that pressure drop  $\Delta P_i = 3\mu_i L V_i / a_i^2$  of fluid  $i$  remains the same with flat and corrugated walls, the apparent average flow velocity  $V_i^*$  of fluid  $i$  must satisfy the condition

$$\frac{V_i^*}{a_i^{*2}} = \frac{V_i}{a_i^2} \Rightarrow V_i^* = V_i \left( \frac{a_i^*}{a_i} \right)^2 = V_i \left( 1 - \frac{\lambda}{a_i} |y_{w,i}^\perp| \right)^2. \quad (51)$$

In this case, the apparent values of  $Pe_i$ ,  $m$ , and  $\xi_L$  are given by

$$Pe_i^* = Pe_i \left( 1 - \frac{\lambda}{a_i} |y_{w,i}^\perp| \right)^3, \quad (52)$$

$$m^* = m \left[ \frac{1 - \frac{\lambda}{a_2} |y_{w,2}^\perp|}{1 - \frac{\lambda}{a_1} |y_{w,1}^\perp|} \right]^4 \Rightarrow m^* k^* = mk \left[ \frac{1 - \frac{\lambda}{a_2} |y_{w,2}^\perp|}{1 - \frac{\lambda}{a_1} |y_{w,1}^\perp|} \right]^3, \quad (53)$$

$$\xi_L^* = \xi_L \left( 1 - \frac{\lambda}{a_1} |y_{w,1}^\perp| \right)^{-4}, \quad (54)$$

and, using (29) and (51) in (37), the overall augmentation heat-transfer number takes the form

$$R_a = \frac{\varepsilon^*}{\varepsilon}. \quad (55)$$

The expressions derived above provide the apparent values  $m^*$ ,  $k^*$ ,  $\kappa_w^*$ , and  $\xi_L^*$  in terms of the parameters of the bulk flow model  $m$ ,  $k$ ,  $\kappa_w$ , and  $\xi_L$  corresponding to a flat heat exchanger, and of the numerically computed values of  $y_{w,i}^\perp$  and  $\overline{\Delta T}$ . These apparent values can then be used in the expressions of the bulk flow model provided in Section 2 to determine the outlet bulk temperature of fluid 1, which provides, in particular, the heat exchanger effectiveness  $\varepsilon^* = \theta_{m1,out}(m^*, k^*, \kappa_w^*, \xi_L^*)$  needed to evaluate  $R_a$  and  $N_a$ . Analytic expressions for  $N_a$  can be easily derived from Eq. (40) by substituting the values of  $a_1^* V_1^* / a_1 V = Pe_1^* / Pe_1$  and  $m^* k^*$  reported in each case, but they have been omitted here for brevity.

## 5. Results and discussion

In this work we shall restrict our attention to the case of flow transverse ( $|\theta_i| = \pi/2$ ) to sinusoidal corrugations ( $\gamma=0$ ,  $y_{w,2}^\perp = -y_{w,1}^\perp$ ) with equal channel half-widths ( $a_1 = a_2$ ). The analysis of other flow configurations is left for future work. Due to the geometrical symmetries of the problem, the apparent channel half-width can be expressed as

$$a_i^* = a_i - \lambda |y_{w,i}^\perp| = a_i \left( 1 - \Lambda |y_{w,i}^\perp| \right) \quad (56)$$

in terms of the single small parameter  $\Lambda = \lambda / a_1 = \lambda / a_2 \ll 1$  representing the dimensionless corrugation wavelength. In this case, the expressions for  $m^*$ ,  $k^*$ ,  $\kappa_w^*$ , and  $\xi_L^*$ , as well as those for the heat-transfer and entropy augmentation numbers  $R_a$  and  $N_a$ , reduce to those given in Table 1.

Table 2 shows the variation of  $\kappa_w^*$  with the dimensionless corrugation amplitude,  $A/2\pi$ , the dimensionless wall thickness,  $\Delta_w$ , and the wall-to-fluid and fluid-to-fluid heat conductivity ratios,  $K_w$  and  $K$ . The results are presented in terms of the ratio  $\kappa_w^* / \kappa_w = (1 - \Lambda |y_{w,1}^\perp|) / \overline{\Delta T}$ , with  $\kappa_w^*$  expressed as percentage of its reference value  $\kappa_w = (k_w / \delta_w)(a_1 / k_1)$  for a flat wall of finite thickness,  $\delta_w$ , and thermal conductivity,  $k_w$ . Different wall designs and conductivity ratios are

Constant flow rate ( $n = 0$ )	Constant pumping power ( $n = 3/2$ )	Constant pressure drop ( $n = 3$ )
	$m^* = m \left( = \frac{Pe_2}{Pe_1} \right)$	
	$k^* = k \left( = \frac{k_2}{k_1} \equiv K \right)$	
	$\kappa_w^* = \kappa_w (1 - \Lambda  y_{w,1}^\perp ) \frac{1}{\Delta T}$ with $\kappa_w = \frac{K_w}{\Lambda \Delta_w}$	
	$\xi_L^* = \xi_L (1 - \Lambda  y_{w,1}^\perp )^{-(n+1)}$	
	$R_a = (1 - \Lambda  y_{w,1}^\perp )^{3-n} \frac{\varepsilon^*}{\varepsilon}$	
	$N_a = \frac{\ln \left[ \left( 1 + \varepsilon^* \frac{\Delta T}{T_{1,in}} \right) \left( \frac{1}{1 + \Delta T / T_{1,in}} \right)^{mk} \left( 1 + \left( 1 - \frac{\varepsilon^*}{mk} \right) \frac{\Delta T}{T_{1,in}} \right)^{mk} \right]}{\ln \left[ \left( 1 + \varepsilon \frac{\Delta T}{T_{1,in}} \right) \left( \frac{1}{1 + \Delta T / T_{1,in}} \right)^{mk} \left( 1 + \left( 1 - \frac{\varepsilon}{mk} \right) \frac{\Delta T}{T_{1,in}} \right)^{mk} \right]} (1 - \Lambda  y_{w,1}^\perp )^n$	

**Table 1.** Expressions determining the apparent values of  $m^*$ ,  $k^*$ ,  $\kappa_w^*$  and  $\xi_L^*$  to be used in the bulk flow model to evaluate the effect of the wall corrugations in the case of flow transverse ( $|\theta_i| = \pi/2$ ) to sinusoidal corrugations ( $\gamma = 0$ ,  $y_{w,2}^\perp = -y_{w,1}^\perp$ ) with equal channel half-widths ( $a_1 = a_2$ ). Also given are the expressions for the heat-transfer and entropy augmentation numbers  $R_a$  and  $N_a$ .

considered, ranging from low to moderate amplitudes and from low- to high-conductive materials. For these and all subsequent calculations, the dimensionless corrugation wavelength has been set equal to  $\Lambda = \lambda / a_i = 0.25 \ll 1$ .

The results shown in Table 2 indicate that the effect of the corrugations is almost invariably to reduce the apparent wall conductivity  $\kappa_w^*$  (i.e., to increase the wall thermal resistance  $1 / \kappa_w^*$ ). This effect is accentuated for highly conductive walls ( $\Delta_w \ll 1$ ,  $K_w \gg 1$ ) with moderately large corrugation amplitudes ( $A \sim 1$ ), when the quasi-stagnant low-conductive recirculating flow established in the corrugation troughs acts as an effective barrier to heat transfer. By contrast, for poorly conductive walls ( $\Delta_w = 0.1$ ,  $K_w \ll 1$ ) the recirculating fluids have significantly larger conductivity than the wall itself and the wall thermal resistance remains virtually unaffected, showing a small reduction as the corrugation amplitude is increased.

Table 3 shows the effect of the dimensionless corrugation amplitude,  $A/2\pi$ , on the apparent dimensionless heat-exchanger length  $\xi_L^*$ . The results are presented in terms of the ratio  $\xi_L^* / \xi_L$  and also as percentage increment of the flat wall value  $\xi_L$  for the three cases under study. As can be seen, the presence of the corrugations always increases the apparent dimensionless heat-exchanger length  $\xi_L^* = L / a_1^* Pe_1^*$  due to the simultaneous reduction of  $a_1^*$  and  $Pe_1^*$  (except in the case of constant flow rate), with larger increments corresponding to larger corrugation amplitudes under the constraint of constant pressure drop.

$\kappa_w^* / \kappa_w$		$A = 0.25$			$A = 0.5$			$A = 1$			
		$K$			$K$			$K$			
		0.5	1	2	0.5	1	2	0.5	1	2	
$\Delta_w = 0.1$	$K_w$	100	6.6%	9.5%	12.2%	2.1%	3.1%	4.0%	0.9%	1.3%	1.7%
		10	38.0%	46.5%	52.8%	15.3%	20.2%	24.5%	6.4%	8.6%	10.6%
		1	82.0%	86.6%	89.9%	56.3%	64.6%	71.5%	30.6%	38.0%	46.0%
		0.1	98.6%	99.4%	99.9%	95.2%	98.0%	99.8%	87.5%	95.2%	100.3%
$\Delta_w = 0.05$	$K_w$	100	3.3%	4.8%	6.2%	1.0%	1.5%	1.9%	0.4%	0.6%	0.8%
		10	21.7%	27.7%	33.1%	7.4%	9.9%	12.4%	2.8%	3.8%	4.8%
		1	67.4%	74.5%	80.2%	36.8%	45.0%	53.2%	16.4%	21.4%	27.6%
		0.1	95.9%	97.5%	98.5%	87.0%	91.8%	95.0%	69.4%	79.3%	87.1%
$\Delta_w = 0.025$	$K_w$	100	1.6%	2.4%	3.0%	0.5%	0.7%	0.9%	0.2%	0.3%	0.4%
		10	11.0%	14.5%	18.2%	3.4%	4.6%	5.9%	1.2%	1.6%	2.1%
		1	49.5%	58.1%	65.9%	21.6%	27.9%	35.2%	8.4%	11.3%	15.4%
		0.1	91.2%	94.0%	95.9%	74.4%	81.6%	86.8%	49.3%	59.6%	69.1%

**Table 2.** Variation of the normalized ratio  $\kappa_w^* / \kappa_w = (1 - \Lambda |y_{w,1}^\perp|) / \overline{\Delta T}$  (expressed as %) with the dimensionless corrugation amplitude,  $A/2\tau$ , the dimensionless wall thicknesses,  $\Delta_w$ , and the fluid-to-fluid and wall-to-fluid conductivity ratios,  $K$  and  $K_w$ , for fixed values of  $\gamma = 0$ ,  $Pr_i = 5$ ,  $Re_i = 0$ , and  $\Lambda = 0.25$ . The apparent wall positions corresponding to  $A = [0.25, 0.5, 1]$  are  $y_{w2}^\perp = -y_{w1}^\perp = [0.0095, 0.0339, 0.1013]$ .

$\xi_L^* / \xi_L = [1 - (\lambda/a_1)  y_{w,1}^\perp ]^{-(n+1)}$	$A = 0,25$		$A = 0,5$		$A = 1$	
	Value	% Change	Value	% Change	Value	% Change
i) Constant flow rate ( $n = 0$ )	1,0024	+0,24%	1,0091	+0,91%	1,0270	+2,70%
ii) Constant pumping power ( $n = 3/2$ )	1,0060	+0,60%	1,0230	+2,30%	1,0690	+6,90%
iii) Constant pressure drop ( $n = 3$ )	1,0096	+0,96%	1,0370	+3,70%	1,1126	+11,26%

**Table 3.** Variation of the ratio  $\xi_L^* / \xi_L$  (expressed both in absolute value and in percentage change) with the dimensionless corrugation amplitude,  $A$ , for the three cases under consideration.

As previously discussed, use of the computed values of  $\kappa_w^*$  and  $\xi_L^*$  as input parameters for the bulk flow model yields the effectiveness  $\varepsilon^*$  of the corrugated wall heat exchanger for given values of  $m$ ,  $k$ ,  $\kappa_w$  ( $= K_w/\Lambda\Delta_w$ ),  $\xi_L$ ,  $\Lambda$ ,  $Re_{ti}$  ( $= 1.5\Lambda^2 Re_i$ ),  $Pr_i$ ,  $A$ ,  $\Delta_w$ ,  $K_w$  and  $K$  ( $= k$ ). This procedure allows to evaluate the augmentation heat transfer and entropy generation numbers,  $R_a$  and  $N_{av}$ , thereby providing a methodology that could be used to optimize the heat exchanger performance from both an energy and/or an entropy (i.e., energy devaluation [30]) point of view.

Table 4 shows preliminary results corresponding to corrugated walls with different parameter sets. The results indicate that in most situations the corrugations increase the heat exchanger effectiveness  $\varepsilon^*/\varepsilon > 1$ , although the overall heat transfer rate is reduced due to the significant reduction in volume flow rate, making  $\varepsilon^*Q_1/(\varepsilon Q_1)_{\text{flat}} < 1$ . It is interesting to note that the augmentation heat transfer parameter  $R_a$  is smaller than one with constant flow rate, but grows above unity when the flow rate is reduced (e.g., constant pumping power or constant pressure drop). Note also that the improvement in  $R_a$  is accompanied by a reduction in entropy generation rate  $N_{av}$  which is almost unaffected ( $N_a \cong 1$ ) under constant flow rate, but takes values smaller than unity for constant pumping power ( $N_a \cong 0.95$ ) and constant pressure drop ( $N_a \cong 0.9$ ) conditions. These results confirm the ability of the multi-scale asymptotic analysis developed here to provide useful estimations of the heat exchanger performance. This method could therefore be used in future work to perform a thermodynamic optimization of the heat exchanger in terms of the different parameters involved in the model.

(a) Ref. Case	Flat wall	Corrugated wall - A = 1, $Re_{ci} = 0$ , $K_w = 0.1$		
$\varepsilon_{\text{flat}}$	<b>0.7831</b>	Constant flow rate	Constant pumping power	Constant pressure drop
$m \& m^*$	<b>1</b>		1	
$k \& k^*$	<b>2</b>		2	
$\kappa_w \& \kappa_w^*$	<b>4</b>		4.0141	
$\xi_L \& \xi_L^*$	<b>1</b>	1.0260	1.0662	1.1081
$Q_1/Q_{1\text{flat}}$	<b>1</b>	1.0000	0.9623	0.9259
$\varepsilon^*/\varepsilon_{\text{flat}}$	<b>1</b>	1.0090	1.0219	1.0346
$\varepsilon Q_1/(\varepsilon Q_1)_{\text{flat}}$	<b>1</b>	1.0090	0.9833	0.9580
$\Delta P_1 Q_1/(\Delta P_1 Q_1)_{\text{flat}}$	<b>1</b>	1.0800	1.0000	0.9259
$R_a$	<b>1</b>	0.9343 (-6.57%)	0.9833 (-1.67%)	1.0346 (+3.46%)
$N_a$	<b>1</b>	0.9961 (-0.39%)	0.9528 (-4.72%)	0.9109 (-8.91%)
(b) Effect of $K_w$	Flat wall	Corrugated wall - A = 1, $Re_{ci} = 0$ , $K_w = 10$		
$\varepsilon_{\text{flat}}$	<b>0.8562</b>	Constant flow rate	Constant pumping power	Constant pressure drop
$m \& m^*$	<b>1</b>		1	
$k \& k^*$	<b>2</b>		2	
$\kappa_w \& \kappa_w^*$	<b>400</b>		42.4926	
$\xi_L \& \xi_L^*$	<b>1</b>	1.0260	1.0662	1.1081
$Q_1/Q_{1\text{flat}}$	<b>1</b>	1.0000	0.9623	0.9259

$\varepsilon^*/\varepsilon_{flat}$	1	0.9992	1.0091	1.0187
$\varepsilon Q_1/(\varepsilon Q_1)_{flat}$	1	0.9992	0.9710	0.9432
$\Delta P_1 Q_1/(\Delta P_1 Q_1)_{flat}$	1	1.0800	1.0000	0.9259
$R_a$	1	0.9252 (-7.48%)	0.9710 (-2.90%)	1.0187 (+1.87%)
$N_a$	1	1.0006 (+0.06%)	0.9553 (-4.47%)	0.9117 (-8.83%)
<b>(c) Effect of <math>K_w</math></b>	<b>Flat wall</b>	<b>Corrugated wall - <math>A = 1, Re_{ci} = 0, K_w = 100</math></b>		
$\varepsilon_{flat}$	<b>0.8569</b>	Constant flow rate	Constant pumping power	Constant pressure drop
$m \& m^*$	<b>1</b>		<b>1</b>	
$k \& k^*$	<b>2</b>		<b>2</b>	
$\kappa_w \& \kappa_w^*$	<b>4000</b>		<b>66.4740</b>	
$\xi_L \& \xi_L^*$	<b>1</b>	1.0260	1.0662	1.1081
$Q_1/Q_{1flat}$	1	1.0000	0.9623	0.9259
$\varepsilon^*/\varepsilon_{flat}$	1	1.0014	1.0111	1.0207
$\varepsilon Q_1/(\varepsilon Q_1)_{flat}$	1	1.0014	0.9729	0.9451
$\Delta P_1 Q_1/(\Delta P_1 Q_1)_{flat}$	1	1.0800	1.0000	0.9259
$R_a$	1	0.9272 (-7.28%)	0.9729 (-2.71%)	1.0207 (+2.07%)
$N_a$	1	0.9989 (-0.11%)	0.9535 (-4.65%)	0.9101 (-8.99%)
<b>(d) Effect of <math>A</math></b>	<b>Flat wall</b>	<b>Corrugated wall - <math>A = 0.5, Re_{ci} = 0, K_w = 0.1</math></b>		
$\varepsilon_{flat}$	<b>0.7831</b>	Constant flow rate	Constant pumping power	Constant pressure drop
$m \& m^*$	<b>1</b>		<b>1</b>	
$k \& k^*$	<b>2</b>		<b>2</b>	
$\kappa_w \& \kappa_w^*$	<b>4</b>		<b>4.2081</b>	
$\xi_L \& \xi_L^*$	<b>1</b>	1.0085	1.0215	1.0346
$Q_1/Q_{1flat}$	1	1.0000	0.9873	0.9748
$\varepsilon^*/\varepsilon_{flat}$	1	1.0073	1.0116	1.0159
$\varepsilon Q_1/(\varepsilon Q_1)_{flat}$	1	1.0073	0.9988	0.9903
$\Delta P_1 Q_1/(\Delta P_1 Q_1)_{flat}$	1	1.0259	1.0000	0.9748
$R_a$	1	0.9819 (-1.81%)	0.9988 (-0.12 %)	1.0159 (+1.59%)
$N_a$	1	0.9969 (-0.31%)	0.9823 (-1.77%)	0.9679 (-3.21 %)
<b>(e) Effect of <math>A</math></b>	<b>Flat wall</b>	<b>Corrugated wall - <math>A = 1.5, Re_{ci} = 0, K_w = 0.1</math></b>		

$\varepsilon_{flat}$	0.7831	Constant flow rate	Constant pumping power	Constant pressure drop
$m \& m^*$	1		1	
$k \& k^*$	2		2	
$\kappa_w \& \kappa_w^*$	4		5.5132	
$\xi_L \& \xi_L^*$	1	1.0459	1.1187	1.1966
$Q_1/Q_{1flat}$	1	1.0000	0.9349	0.8741
$\varepsilon^*/\varepsilon_{flat}$	1	1.0395	1.0607	1.0810
$\varepsilon Q_1/(\varepsilon Q_1)_{flat}$	1	1.0395	0.9917	0.9449
$\Delta P_1 Q_1/(\Delta P_1 Q_1)_{flat}$	1	1.1441	1.0000	0.8741
$R_a$	1	0.9086 (-9.14%)	0.9917 (-0.83 %)	1.0810 (+8.10%)
$N_a$	1	0.9813 (-1.87%)	0.9063 (-9.37%)	0.8363 (-16.37 %)
<b>(f) Effect of <math>Re_{ci}</math></b>	<b>Flat wall</b>	<b>Corrugated wall - <math>A = 1, Re_{ci} = 64, K_w = 0.1</math></b>		
$\varepsilon_{flat}$	0.7831	Constant flow rate	Constant pumping power	Constant pressure drop
$m \& m^*$	1		1	
$k \& k^*$	2		2	
$\kappa_w \& \kappa_w^*$	4		4.0351	
$\xi_L \& \xi_L^*$	1	1.0270	1.0690	1.1126
$Q_1/Q_{1flat}$	1	1.0000	0.9608	0.9231
$\varepsilon^*/\varepsilon_{flat}$	1	1.0098	1.0232	1.0363
$\varepsilon Q_1/(\varepsilon Q_1)_{flat}$	1	1.0098	0.9831	0.9566
$\Delta P_1 Q_1/(\Delta P_1 Q_1)_{flat}$	1	1.0833	1.0000	0.9231
$R_a$	1	0.9321 (-6.79%)	0.9831 (-1.69 %)	1.0363 (+3.63%)
$N_a$	1	0.9957 (-0.43%)	0.9507 (-4.93%)	-0.9073 (-9.27 %)

**Table 4.** (a)(b)(c): Influence of the wall-to-fluid heat conductivity ratio,  $K_w = [0.1, 10, 100]$ ; (d)(a)(e): influence of the dimensionless corrugation amplitude,  $A = [0.5, 1, 1.5]$ ; and (a)(f): influence of the Reynolds number,  $Re_{ci} = [0, 64]$ , on the performance of laminar counterflow parallel-plate heat exchangers with small scale-wall corrugations. In all reported cases  $Pr_i = 5$ ,  $\Lambda = 0.25$ ,  $\Delta_w = 0.1$ , and  $K = 2$ .

## 6. Conclusion

Laminar counterflow parallel-plate heat exchangers with small-scale wall corrugations have been studied theoretically and numerically following a multi-scale asymptotic approach. The

analysis assumes that the corrugation wavelength and amplitude are comparable to each other but are much smaller than the channel half-width. In this case, the problem exhibits two main asymptotic regions: a bulk flow region where the walls appear flat at leading order, and where axial heat conduction can be neglected in first approximation provided the Peclet numbers are large enough, and a near-wall region where a full interaction exists between heat convection and conduction in the fluids, coupled by transverse and longitudinal conduction in the thin corrugated wall.

In the bulk flow region, an approximated semi-analytical two-term solution based on eigenfunction expansions provides accurate predictions of the outlet fluid temperatures in terms of the bulk parameters  $m$ ,  $k$ ,  $\kappa_w$ , and  $\xi_L$ .

The heat transfer process in the near wall region is investigated numerically by specifying the overall heat flux transverse to the wall and calculating the apparent wall temperature jump seen by the outer bulk flow. The numerical solution, based on a boundary fitted finite difference method, involves the parameters  $Re_{i,r}$ ,  $Pr_i$ ,  $K$ ,  $K_w$ ,  $\Delta_w$ ,  $\theta_i$ , as well as the corrugation shape, defined here by  $A$  and  $\gamma$ . The analysis shows that, far from the wall, the effect of the corrugations is similar to that of a thickened virtual plane surface with an appropriately defined apparent thermal resistance.

Although for sufficiently large Reynolds numbers the flow in the channels and past the corrugations is known to become unstable and undergo transition to a self-sustained oscillatory and later turbulent regime [31,32] resulting in enhanced heat transfer rates, this study has focused on the role of the wall corrugations on the overall heat transfer process before this transition occurs.

The effect of the corrugations is incorporated into the bulk flow model defining apparent values of the bulk flow parameters  $m^*$ ,  $k^*$ ,  $\kappa_w^*$  and  $\xi_L^*$  in terms of those of the originally flat wall. Three different constraints have been considered for the determination of the apparent parameters: i) constant flow rate, ii) constant pumping power, and iii) constant pressure drop. The results, restricted to the case of sinusoidal wall geometries ( $\gamma = 0$ ) with equal channel half-widths ( $a_1 = a_2$ ) show that the most relevant parameter determining the effect of the corrugations is the wall thermal conductivity  $K_w$ . For highly conductive (e.g., metallic) walls, the addition of the corrugations always leads to a reduced wall conductivity  $\kappa_w^*$  (or an increased wall thermal resistance,  $1/\kappa_w^*$ ). On the other hand, for poorly conductive (e.g., polymeric) walls, the addition of the corrugations may lead to a slightly larger apparent wall conductivity  $\kappa_w^*$  (or a smaller wall thermal resistance) under certain flow conditions, particularly for relatively thick walls and large corrugation amplitudes.

The aim of this work has been to introduce the methodology followed by the multi-scale asymptotic analysis and to present preliminary calculations that illustrate the type of results that can be obtained with the most simple geometry and flow conditions. Corrugations of different shapes, involving for instance scalloped geometries,  $\gamma \neq 0$ , with different channel half widths,  $a_1 \neq a_2$ , remain underexplored and warrant future work.

## Acknowledgements

This work was supported by Project ENE2011-24574 of Spanish *Ministerio de Economía y Competitividad*.

## Author details

Marcos Vera and Alberto E. Quintero

\*Address all correspondence to: marcos.vera@uc3m.es

Department of Thermal and Fluids Engineering, Universidad Carlos III de Madrid, Leganés, Spain

## References

- [1] Hardt S, Ehrfeld W, Hessel V. Strategies for size reduction of microreactors by heat transfer enhancement effects. *Chem. Eng. Commun.* 2003;(190): 540-559.
- [2] Esarte J, Min G, Rowe DM. Modelling heat exchangers for thermoelectric generators. *J. Power Sources.* 2001;(93): 72-76.
- [3] Yu J, Zhao H. A numerical model for thermoelectric generator with the parallel-plate heat exchanger. *J. Power Sources.* 2007;(172): 428-434.
- [4] Wakeland RS, Keoliana RM. Effectiveness of parallel-plate heat exchangers in thermoacoustic devices. *J. Acoust. Soc. Am.* 2004;(115): 2873-2886.
- [5] Marquardt ED, Radebaugh R. Compact high effectiveness parallel plate heat exchangers. In Ross Jr. RG, editor. *Cryocoolers 12*. R.G. Ross Jr. ed.: Kluwer Academic/Plenum Publishers; 2003. 507-516.
- [6] Nellis GF. A heat exchanger model that includes axial conduction, parasitic heat loads, and property variations. In *Cryogenics 43*; 2003. 523-538.
- [7] Radebaugh R. Microscale heat transfer at low temperatures. In Kakaç S, Vasiliev LL, Bayazitoğlu Y, Yener Y, editors. *Microscale Heat Transfer Fundamentals and Applications*.: Springer Netherlands 93-124.
- [8] Shah RK, London AL. *Laminar Flow Forced Convection in Ducts: A Source Book for Compact Heat Exchanger Analytical Data: A Source Book for Compact Heat Exchanger Analytical Data*. New York: Academic Press; 1978.

- [9] Nunge RJ, Gill WN. Analysis of heat or mass transfer in some countercurrent flows. *Int. J. Heat Mass Tran.* 1965; 8(6): 873-886.
- [10] Nunge RJ, Gill WN. An analytical study of laminar counterflow double-pipe heat exchangers. *A. I. Ch. E. Journal.* 1966; 12(2): 279-289.
- [11] Papoutsakis E, Ramkrishna D. Conjugated Graetz problems - II: Fluid-fluid problems. *Chem. Eng. Sci.* 1981; 36(8): 1393-1399.
- [12] Vera M, Liñan A. Laminar counterflow parallel-plate heat exchangers: Exact and approximate solutions. *Int. J. Heat Mass Tran.* 2010; 36(8): 1393-1399.
- [13] Webb RL, Kim NH. *Principles of enhanced heat transfer.* New York: Taylor & Francis; 1994.
- [14] Moffatt HK. Viscous and resistive eddies near a sharp corner. *Journal of Fluid Mechanics.* 1964; 18(1): 1-18.
- [15] Sunden B, Trollheden S. Periodic laminar flow and heat transfer in a corrugated two-dimensional channel. *Int. Commun. Heat Mass.* 1989; 16(2): 215-225.
- [16] Fabbri G. Heat transfer optimization in corrugated wall channels. *International Journal of Heat and Mass Transfer.* 2000; 43: 4299-4310.
- [17] Durmuş A, Benli H, Kurtbaş İ, Gül H. Investigation of heat transfer and pressure drop in plate heat exchangers having different surface profiles. *International Journal of Heat and Mass Transfer.* 2009; 52: 1451-1457.
- [18] Vera M, Liñan A. Exact solution for the conjugate fluid-fluid problem in the thermal entrance region of laminar counterflow heat exchangers. *International Journal of Heat and Mass Transfer.* 2011; 54(1): 490-499.
- [19] Quintero AE, Vera M, Rivero-de-Aguilar B. Wall conduction effects in laminar counterflow parallel-plate heat exchangers. *International Journal of Heat and Mass Transfer.* 2014; 70: 939-953.
- [20] Woollard HF, Billingham J, Jensen OE, Lian G. A multi-scale model for solute transport in a wavy-walled channel. *J. Eng. Math.* 2009; 64(1): 25-48.
- [21] Hocking LM. A moving fluid interface on a rough surface. *J. Fluid Mech.* 1976; 76(4): 801-817.
- [22] Wang CY. Drag due to a striated boundary in slow Couette flow. *Phys. Fluids.* 1978; 21: 697-698.
- [23] Orszag SA, Kells LC. Transition to turbulence in plane Poiseuille and plane Couette flow. *J. Fluid Mech.* 1980; 96(1): 159-205.
- [24] Richardson S. On the no-slip boundary condition. *Journal of Fluid Mechanics.* 1973; 59(04): 707-719.

- [25] Luccini P, Manzo F, Pozzi A. Resistance of a grooved surface to parallel flow and cross-flow. *J Fluid Mech.* 1991; 228: 87-109.
- [26] Bejan A. General criterion for rating heat-exchanger performance. *International Journal of Heat and Mass Transfer.* 1978; 21: 655-658.
- [27] Bejan A. Entropy generation minimization: The new thermodynamics of finite-size devices and finite-time processes. *Journal of Applied Physics.* 1996; 79(3): 1191-1218.
- [28] Bejan A. Entropy generation minimization: The method of thermodynamic optimization of finite-size systems and finite-time processes. Boca Raton: CRC Press; 1996.
- [29] Bejan A. Second law analysis in heat transfer. 1980; 5(8): 720-732.
- [30] Wenterodt T, Herwig H. The entropic potential concept: a new way to look at energy transfer operations. *entropy.* 2014; 16: 2071-2084.
- [31] Stone K, Vanka SP. Numerical study of developing flow and heat transfer in a wavy passage. *Journal of Fluids Engineering (Transactions of ASME).* 1999; 121(4): 713-719.
- [32] Hossain MZ, Sadrul Islam AKM. Numerical Investigation of fluid flow and heat transfer characteristics in sine, triangular and arc-shaped channels. *Thermal Science.* 2007; 11(1): 17-26.